Published in final edited form as:

Mol Cancer Res. 2017 June ; 15(6): 723–734. doi:10.1158/1541-7786.MCR-16-0338.

Hypoxia Selectively Enhances Integrin Receptor Expression to Promote Metastasis

Julia A. Ju[1,5,6], **Inês Godet**[1,5,6], **I Chae Ye**[1,5], **Jungmin Byun**[5], **Hasini Jayatilaka**[5], **Sun Joo Lee**[2,3], **Lisha Xiang**[3], **Debangshu Samanta**[2,3], **Meng Horng Lee**[5], **Pei-Hsun Wu**[5], **Denis Wirtz**[1,5], **Gregg L. Semenza**[1,2,3,4], and **Daniele M. Gilkes**[1,5,*]

[1]Department of Oncology, The Sidney Kimmel Comprehensive Cancer Center, The Johns Hopkins University School of Medicine, Baltimore, MD, USA

[2]Vascular Program, Institute for Cell Engineering, Johns Hopkins University School of Medicine Baltimore, MD 21205, USA

[3]McKusick-Nathans Institute of Genetic Medicine, Johns Hopkins University School of Medicine Baltimore, MD 21205, USA

[4]Departments of Pediatrics, Medicine, Radiation Oncology, and Biological Chemistry, Johns Hopkins University School of Medicine Baltimore, MD 21205, USA

[5]Department of Chemical and Biomolecular Engineering, The Johns Hopkins University, Baltimore, Maryland 21218, USA

Abstract

Metastasis is the leading cause of breast cancer (BCa) mortality. Previous studies have implicated hypoxia-induced changes in the composition and stiffness of the extracellular matrix (ECM) in the metastatic process. Therefore, the contribution of potential ECM binding receptors in this process was explored. Using a bioinformatics approach the expression of all integrin receptor subunits, in two independent BCa patient data sets, were analyzed to determine if integrin status correlates with a validated hypoxiainducible gene signature. Subsequently, a large panel of breast cancer cell lines were used to validate that hypoxia induces the expression of integrin's that bind to collagen (ITGA1, ITGA11, ITGB1) and fibronectin (ITGA5, ITGB1). Hypoxia-inducible factors (HIF-1 and HIF-2) are directly required for ITGA5 induction under hypoxic conditions, which leads to enhanced migration and invasion of single cells within a multicellular 3D tumor spheroid but did not affect migration in a 2D microenvironment. ITGB1 expression requires HIF-1α, but not HIF-2α, for hypoxic induction in breast cancer cells. ITGA5 (α5 subunit) is required for metastasis to lymph nodes and lungs in breast cancer models and high ITGA5 expression in clinical biopsies is associated with an increased risk of mortality.

Implications—These results reveal that targeting ITGA5 using inhibitors that are currently under consideration in clinical trials may be beneficial for patients with hypoxic tumors.

*Correspondence: Dr DM Gilkes, Breast and Ovarian Cancer Program, The Johns Hopkins Sidney Kimmel Comprehensive Cancer Center, 1650 Orleans St, Suite 152, Baltimore, MD 21231, USA. dgilkes1@jhu.edu.

[6]Authors contributed equally to this work

The authors declare no conflict of interest.

Keywords

ITGA5; ITGB1; hypoxia; HIF-1; collagen; fibronectin; integrins

Introduction

Increased cell proliferation and oxygen consumption result in lower oxygen availability in solid tumors as compared to normal tissue (1,2). Intratumoral hypoxia has been associated with invasion, metastasis, treatment failure, and patient mortality (3,4). Cancer cells survive and adapt to hypoxic conditions, in part, through the activation of hypoxia-inducible factor 1 (HIF-1) and HIF-2, which induce the expression of gene products involved in angiogenesis, glucose utilization, invasion, and metastasis (5). HIF-1 is a heterodimeric protein composed of a constitutively expressed HIF-1β subunit and an O_2-regulated HIF-1α subunit (6,7). In mouse models, inhibition of HIF expression impedes breast cancer growth, angiogenesis, and metastasis (8-12). In human breast cancer biopsies, increased HIF-1α protein levels are associated with an increased risk of metastasis and mortality (13-17). Our previous work implicated hypoxia in alterations of the composition and stiffness of the intratumoral extracellular matrix (ECM), which promoted metastasis (18-20). The ECM provides intracellular signaling cues and also provides contact points for cell migration. Specific cell-ECM interactions are critical for cell survival and altered cell-matrix adhesion is a classic hallmark of neoplasia (21,22). We hypothesized that hypoxia could coordinately induce both ECM alterations and the expression of integrins that interact with the altered ECM (23). The major constituents of the ECM are collagens, elastin, fibronectin and laminins. Collagen is the most abundant fibrous protein within the interstitial ECM. Fibronectin is required for ECM organization and fibrillogenesis and mediates cell attachment. Integrin dimers, as well as discoidin domain receptors, and syndecans mediate adhesion to the ECM (24,25).

Twenty-four distinct integrin heterodimers are expressed in mammals as a result of combinatorial association of 18 α and 8 β subunits. ECM ligands bind to the α subunit and activate intracellular signaling events via the β subunit to integrate extracellular and intracellular events necessary for cell motility and invasion (26,27). Integrin expression patterns are cell-type specific and vary with microenvironmental context (26,27). Many integrins are expressed at low or undetectable levels in adult epithelia, but are upregulated in tumors (28). Integrins expressed in epithelia include several β1 integrins ($\alpha_1\beta_1$, $\alpha_2\beta_1$, $\alpha_3\beta_1$, $\alpha_5\beta_1$, $\alpha_6\beta_1$, and $\alpha_9\beta_1$), $\alpha_6\beta_4$, $\alpha_v\beta_5$, and $\alpha_v\beta_6$ (29).

Hypoxia has been shown to enhance ITGB1 (integrin β_1) expression in fibroblasts(30), $\alpha_5\beta_1$ and $\alpha_v\beta_5$ in endothelial cells (31), $\alpha_v\beta_3$ in melanoma cells (32), β_2 expression in leukocytes (33,34), and α_5 expression in colon cancer cells (35). In human mesenchymal stem cells, hypoxia induces the expression of various integrins (α_1, α_3, α_6, α_{11}, α_v, β_1, β_3) (36). Our goal was to determine how hypoxia regulates integrin expression in human breast cancer and to investigate whether targeting integrin receptors might be an effective method for blocking the metastatic response potentiated by changes to the ECM during tumor progression. Several integrin inhibitors are advancing through clinical trials with positive clinical findings

(28). To date, no study has investigated the induction of each individual integrin subunit in a large cohort of patients and/or in a large panel of breast cancer cell lines.

In order to determine if patients with highly hypoxic tumors might benefit from blocking integrin receptors and in order to determine the integrin subunit(s) that would be suitable as a means to target hypoxic cells, we examined a large cohort of breast cancer patients and a panel of 20 well characterized cell lines for integrin expression. Initially, we utilized a bioinformatics approach and interrogated two datasets: The Cancer Genome Atlas (TCGA) (37) and the Gene Expression-Based Outcome for Breast Cancer Dataset (GOBO) (38) and identified candidate integrins that might be induced under hypoxic conditions based on a significant correlation of their expression pattern in human breast cancers with that of known HIF target genes. The results were confirmed using a panel of 20 breast cancer cell lines exposed to hypoxic conditions. Expression of integrin α_5 subunit (ITGA5) was uniquely hypoxia-induced in 19 of the 20 cell lines assayed and had the strongest correlation with the HIF gene signature. HIFs were required for transcriptional activation of the *ITGA5* gene. Surface expression of the $\alpha_5\beta_1$ receptor was required for 3D cell migration and migration of cells within a multicellular spheroid, but surprisingly did not alter 2D cell migration. Inhibition of $\alpha_5\beta_1$ expression abrogated invasion and motility of cells within a spheroid embedded in a collagen and fibronectin matrix. Importantly, inhibition of $\alpha_5\beta_1$ expression decreased metastasis in mouse models of breast cancer suggesting that α_5 inhibition may be an effective treatment strategy for breast cancer patients.

Materials and methods

Cell culture

All cell lines except SUM159 and SUM149 were obtained from the ATCC and cultured as described by the ATCC. The SUM149 and SUM159 cells were gifts from the Sukumar lab and were authenticated by STR sequencing and confirmed to be mycoplasma free. Hypoxic cells were maintained at 37°C in a modular incubator chamber (Billups–Rothenberg) flushed with a gas mixture containing 1% O_2, 5% CO_2, and 94% N_2.

Animal studies

Female 5- to 7-week-old NOD-SCID or BALB/c (Charles River Laboratories) mice were used according to protocols approved by the Johns Hopkins University Animal Care and Use Committee. Mice were anesthetized, and 2×10^6 MDA-MB-231 cells or 5×10^5 4T1 cells were injected into the mammary fat pad. Tumors were measured in three dimensions (a, b, and c), and volume (V) was calculated as $V = abc \times 0.52$. Tumors, ipsilateral axillary lymph nodes, and lungs were harvested, formalin fixed, paraffin embedded and used for IHC staining. Lung tissue was used to isolate genomic DNA for qPCR to quantify human HK2 and mouse 18S rRNA gene sequences.

Immunoblot assays

Aliquots of whole cell lysates were prepared in NP-40 buffer (150 mM NaCl, 1% NP-40, 50 mM Tris-HCl, pH 8.0) and fractionated by 8% SDS-PAGE. Antibodies against HIF-1α and

ITGA5 (BD Biosciences), HIF-2α (Novus Biologicals), β-actin and ITGB1 (Santa Cruz) were used.

Immunohistochemistry

Paraffin embedded tissue sections were dewaxed and hydrated. LSAB+ System (DAKO) was used for ITGA5, HIF-1α and vimentin IHC staining according to the manufacturer's instructions. Inflated lung sections were stained with hematoxylin and eosin to detect metastatic foci as previously described (11,12). Image analysis of vimentin stained lymph node tissue sections was conducted as previously described (20).

Lentiviral transduction

The pLKO.1-puro lentiviral vectors encoding shRNA targeting human and mouse ITGA5 were purchased from Sigma–Aldrich. The pLKO.1-puro lentiviral vectors encoding shRNA targeting human HIF-1α and HIF-2α were previously described (39). The recombinant vectors were cotransfected with plasmid pCMV-dR8.91 and a plasmid encoding vesicular stomatitis virus G protein into 293T cells using Polyjet. Filtered viral supernatant collected 48 h posttransfection was added to MDA-MB-231 cells with 8 μg/mL polybrene (Sigma–Aldrich). Puromycin (0.5 μg/mL) was added to the medium of cells transduced for selection. Following selection, cells were pooled together for use.

India ink staining of lungs

Mice were euthanized, and India ink (15%) was injected into the lungs through the trachea. The lungs were fixed in Feketet's solution (100 mL of 70% alcohol, 10 mL of formalin, and 5 mL of glacial acetic acid) at room temperature.

Reverse transcription (RT) and qPCR

Total RNA was extracted from cells using TRIzol (Invitrogen) and treated with DNase I (Ambion). One microgram of total RNA was used for first-strand DNA synthesis with the iScript cDNA Synthesis system (BioRad). qPCR was performed using human-specific primers and iTaq SYBR Green Universal Master Mix (Bio-Rad). The expression of each target mRNA relative to 18S rRNA was calculated based on the threshold cycle (Ct) as $2^{-\Delta(\Delta Ct)}$, where $\Delta Ct = Cttarget - Ct_{18S}$ and $\Delta(\Delta Ct) = \Delta Ct_{test} - \Delta Ct_{control}$. Primer sequences are shown in Table S1.

ChIP assay

MDA-MB-231 cells were cross-linked with formaldehyde quenched with glycine and lysed with SDS lysis buffer (1% SDS, 10 mM EDTA and 50 mM Tris, pH 8.1). Chromatin was sheared by sonication and lysates were precleared with salmon sperm DNA/protein A-agarose slurry (Millipore) and incubated with antibody against HIF-1α (Santa Cruz Biotechnology), HIF-1β (Novus Biologicals), or HIF-2α (Novus Biologicals), or with IgG (Santa Cruz Biotechnology or Novus Biologicals) as previously described (40).

Immunofluorescence microscopy

Cells were fixed with 4% formaldehyde and permeabilized with 0.1% (v/v) Triton-X100 and incubated with an antibody against vinculin (Sigma-Aldrich) and integrin α5 (BD Biosciences). Following washes in PBS, cells were incubated with phalloidin (Invitrogen) at 1:150 dilution, anti-mouse Alexa Fluor 488 and anti-rabbit Alexa Fluor 568 antibodies (Life Technologies) at 1:200. Fluorescent images were obtained using a Nikon A1 confocal microscope with 60× oil-immersion lens.

Fluorescence-activated cell sorting (FACS)

Cells were trypsinized, washed with PBS, collected in FACS staining buffer, incubated with Fc Block (BD Biosciences), followed by fluorescent labeling using an allophycocyanin-conjugated antibody against integrin α5β1 (BD Biosciences). Samples were analyzed using a FACScalibur flow cytometer.

Cell migration

Cell culture plates were left uncoated or coated with 10 μg of fibronectin for 2D motility measurements. For 3D migration measurements, collagen matrices were prepared with soluble rat tail type I collagen in acetic acid (Corning) to achieve a final concentration of 1 mg/ml collagen supplemented with 10 or 50 μg/ml of fibronectin. Cell movement over time was imaged using a Cascade 1K CCD camera (Roper Scientific) mounted on a Nikon TE2000E phase contrast microscope equipped with a 10× objective and controlled by NIS-Elements AR imaging software. Images were taken every 5 min for 13 h. Cells in the time-lapse movies were tracked using MetaMorph to calculate x- and y-coordinates at each time interval.

APRW modeling for motility analysis

APRW model analysis was performed as described in detail using Matlab (code available) (41). 2D and 3D cell trajectory data were used to statistically profile cell migration using the mean squared displacement (MSD) which can be obtained from [x(t), y(t)] coordinates of cells with time (t). $MSD(\tau) = [x(t + \tau) - x(t)]^2 + [y(t + \tau) - y(t)]^2$ where τ = 5 min*frame number. Values of persistence and speed are obtained from APRW model fitting and expressed as speed (S) and persistence (P) of cells.

Microarray data analysis

TCGA breast cancer data(37) were obtained from the online data portal (http://tcgadata.nci.nih.gov/tcga/tcgaHome2.jsp). GOBO data were collated from 7 independent studies available in the GEO database and obtained as *.rdata files from the authors (38). Pearson's correlation and Kaplan-Meier analyses were conducted using GraphPad Prism Software.

Spheroid invasion

Cell spheroids were formed in round-bottom 96-well tissue culture plates as described(42). Cells (1×10^4 cells/ml) were resuspended in spheroid formation media, (DMEM and Methocult H4100 (3:1)) and centrifuged at 1800 rpm for 30 min. Following 72-h incubation,

spheroids were embedded into 2 mg/ml collagen containing DMEM and soluble rat tail type I collagen (Corning) with the addition fibronectin (50 μg/mL). Spheroids were imaged using Cytation 5 (Biotek) at 10×.

Results

Correlating integrin expression with a HIF meta-gene signature

We previously reported that hypoxia promotes collagen biogenesis in the hypoxic region of breast tumors by enhancing the transcription of specific enzymes that mediate fibrillar collagen formation (18-20,23). To investigate whether hypoxia alters integrin expression in breast cancer cells, we analyzed gene expression data from two independent databases (TCGA and GOBO) correlating the level of all 18 integrin α and β subunits with a HIF meta-gene signature. The HIF signature was comprised of 9 genes (P4HA1, P4HA2, PLOD1, PLOD2, LOX, LOXL2, ANGPTL4, VEGF, SLC2A1) which were selected based on their level of induction under hypoxia in a panel of breast cancer cells and were prognostic of survival in a retrospective study of breast cancer patients (43) (Fig. S1A). A Pearson's correlation coefficient was calculated for each integrin by comparing the averaged mean-centered expression of each gene in the hypoxia signature with the expression of each integrin subunit (Fig. 1A-B). The correlation coefficient was well matched between the two datasets with *ITGA5* showing the highest correlation with the HIF signature in both TCGA and GOBO data sets (Fig. 1B). We chose to further investigate four genes encoding integrin subunits (*ITGA1, ITGA5*, *ITGA11,* and *ITGB1*) that showed the highest level of correlation with the HIF signature.

We analyzed ITGA1, ITGA5, ITGA11, and ITGB1 mRNA levels in a panel of 20 breast cancer cell lines (in triplicate) following exposure to 20% or 1% O_2 for 24 h (Fig. 1C-F). ITGA5 mRNA levels were significantly induced (Student t-test; $\alpha > 0.05$) by 2-10 fold in 19 out of the 20 cell lines examined (Fig. 1C). ITGA5 mRNA levels were a minimum of 10-fold lower in luminal as compared to basal breast cancer cell lines (Figure 1C). ITGB1 mRNA levels were induced by hypoxia in 12 out of 20 cell lines with modest but reproducible induction of up to 2.5-fold (Fig 1D). ITGA1 (α1 subunit of the α1β1 collagen receptor) and ITGA11 (α11 subunit of the α11β1 collagen receptor) expression was induced in 4 (ITGA1) and 10 (ITGA11) of 20 cell lines (Fig. 1E-F). In most cell lines, ITGA11 mRNA expression was not detectable until cells were exposed to hypoxic conditions.

To exclude the possibility that additional integrins might be induced by hypoxia but were not identified using our bioinformatics approach, we examined the expression of 4 additional integrin subunits that are expressed in epithelial cells but that did not correlate with the HIF signature (*ITGA2*, *ITGA3*, *ITGA4*, *ITGA6*). Exposure to hypoxia did not induce their mRNA expression (Fig. S1B). P4HA1 mRNA levels were used as a positive control for the experiment. Taken together, the analysis suggests that our HIF meta-gene signature is a reasonable method for identifying potential hypoxia inducible genes encoding integrin subunits in breast cancer cells and that ITGA5 is the only integrin subunit robustly expressed across a wide range of breast cancer cells.

Hypoxia induces the expression of ITGA5 and ITGB1 in a HIF-dependent manner

ITGA5 protein expression was increased 1.9 to 2.8 fold in MCF-7, ZR.75.1, MDA-MB-231, and MCF10A cells by exposing cells to hypoxic conditions or by treating cells with dimethyloxallyl glycine (DMOG), a 2-oxoglutarate (2-OG) analog that stabilizes HIF protein levels (Fig. 2A). Immunohistochemical staining of tumors derived from the orthotopic transplantation of MDA-MB-231 cells revealed intense ITGA5 staining in perinecrotic (hypoxic) regions of orthotopic tumors, which co-localized with HIF-1α staining (Fig. 2B). To determine whether HIF-1α or HIF-2α were required for ITGA5 or ITGB1 expression under hypoxic conditions, we generated MDA-MB-231 subclones that were stably transfected with an expression vector encoding a non-targeting control (NTC) short hairpin RNA (shRNA) or expression vector encoding an shRNA targeted against HIF-1α (sh1α) or HIF-2α (sh2α). The hypoxic induction of ITGA5 and ITGB1 mRNA (Fig. 2C-D) and protein (Fig. 2E) expression was blocked when expression of HIF-1α or HIF-2α (for ITGA5 only) was inhibited by shRNA. RNA from tumors generated with MDA-MB-231 subclones expressing sh1α or sh2α also showed decreased ITGA5 and ITGB1 expression compared to tumors generated with the NTC subclone (Fig. 2F-G). MCF-7 subclones expressing sh1α or sh2α (Fig. S2A) were also generated and displayed decreased cell surface expression of α5β1 at 20% and 1% O_2 compared to NTC cells (Fig. 2H and Fig. S2B). Taken together, the results show that HIF-1α and HIF-2α are required for hypoxic induction of *ITGA5* whereas only HIF-1α is required for *ITGB1* induction.

HIF-1 and HIF-2 bind to the *ITGA5* promoter

The human *ITGA5* gene was examined for matches to the consensus HIF binding site sequence 5′-(A/G)CGTG-3′. Three candidate sites were identified and interrogated by chromatin immunoprecipitation (ChIP) assays of MDA-MB-231 cells exposed to 20% or 1% O_2 for 16 h (Fig. 3). Antibodies against HIF-1α, HIF-2α, HIF-1β and rabbit Ig (IgG) were used for ChIP. Site 1 was located 1.0 kb 5′ upstream of the transcriptional start site (Fig. 3A) and showed significant hypoxia-induced binding of HIF-1α, HIF-2α, and HIF-1β (Fig. 3B). Site 2 and Site 3, located within the first intron of *ITGA5* (Fig. 3A), were not bound by HIF-1α, HIF-2α, or HIF-1β (Fig. 3B).

To test whether Site 1 functions as a hypoxia response element (HRE), a 60-bp fragment encompassing Site 1 (Fig. 3A) was inserted downstream of SV40 promoter and a firefly luciferase coding sequences in the reporter plasmid pGL2-promoter. MDAMB-231 cells were co-transfected with pGL2–ITGA5-HRE and pSV-Renilla and exposed to 20% or 1% O_2 for 24 h. Exposure to hypoxic conditions resulted in a significant increase in firefly luciferase activity compared to a reporter plasmid containing a mutated ITGA5 HRE (Fig. 3C). Taken together, the ChIP and reporter data indicated that HIF-1 and HIF-2 bind to Site 1 and activate *ITGA5* transcription under hypoxic conditions.

Decreased α5β1 surface expression reduces breast cancer cell motility

To identify the functional aspects of α5β1 cell surface expression, we generated MDAMB-231 subclones that were stably transfected with a vector encoding either of two different shRNAs targeted against ITGA5 (shA5-1 and shA5-2). Decreased mRNA, protein and cell surface expression of the α5β1 receptor was confirmed for both subclones under

normal as well as hypoxic conditions (Supplementary Fig. S3A-C). To determine if ITGA5 is required for focal adhesion formation, subclones were stained with Alexa Fluor 647-conjugated phalloidin to detect polymerized actin (F-actin) and anti-vinculin antibody to detect focal adhesions. ITGA5 staining confirmed localization of ITGA5 to focal adhesions in control cells and decreased focal adhesion formation in shA5-1 cells (Fig. 4A-B).

Focal adhesion size has been shown to correlate with 2D cancer cell motility (44,45). To determine if ITGA5 expression promotes 2D cancer cell motility, we monitored the motility of NTC and shA5-expressing cells on uncoated or fibronectin-coated surfaces using time-lapse microscopy. Individual (x, y) coordinates were determined for each cell every 5 min for 13 h to construct cell trajectory maps (Fig. 4C). Mean squared displacements of individual cells were calculated and fit to an anisotropic persistent random walk (APRW) model of cell motility (41,46). The cell trajectories were fit to an APRW model of cell motility, to calculate velocity (S) and persistence (P). The parameter S can be interpreted as the rate at which a cell moves, the parameter P, or persistence time, represents a measure of the average time period between significant changes in the direction of movement.

Both velocity and directional persistence are used to calculate diffusivity ($D = S^2P/4$), which describes overall cell movement within a specific time frame. Cell diffusivity and persistence time were increased on fibronectin-coated as compared to uncoated surfaces as has been previously reported, but decreasing the level of ITGA5 expression only moderately decreased cell migration on 2D surfaces (Fig. 4D-E).

Decreased α5β1 surface expression reduces 3D cell migration in collagen as well as single cell migration in a complex multicellular spheroid

The most abundant ECM proteins in mouse metastatic breast tumors are fibronectin (FN) and collagens (47). Collagen is abundant in human breast cancer and collagen organization influences tumor progression (48-50), increased FN also correlates with disease progression and mortality (51). To examine the effect of the ITGA5 knockdown on 3D cell motility, MDA-MB-231 control or knockdown cells were embedded in 3D collagen matrices containing 10 or 50 μg/ml of fibronectin to mimic ECM found in breast cancer. The diffusivity and persistence time of ITGA5 knockdown cells migrating in 3D collagen matrices was decreased compared to control cells (Fig. 5A-D) or cells plated on 2D substrates (Fig. 4C-D). A modest decrease in cell motility was noted for NTC cells migrating in matrices containing 50 μg/ml versus 10 μg/ml of fibronectin which may be the result of a decrease in pore size caused by increasing fibronectin concentrations (Fig. S4A-B).

To determine whether ITGA5 expression can also promote migration within a tumor mass, we generated multicellular spheroids of target cells (NTC, shA5-1, or shA5-2) that were labeled with a red fluorescent carbocyanine tracer and mixed them with non-labelled naive cells at a ratio of 1:10. The multicellular spheroids were embedded into collagen gels containing 50 μg/mL of fibronectin. This allowed individually labeled NTC, shA5-1, or shA5-2 cell trajectories to be monitored over a 15 h time course at single cell resolution (Fig. 5E). The results demonstrate that decreasing ITGA5 expression reduces the diffusivity and persistence time of cells migrating within a multicellular spheroid mass (Fig. 5F-G).

To examine the role of ITGA5 in invasion at the edge of a multicellular spheroid, we generated spheroids of NTC or shA5 cells and embedded them in collagen gels containing 50 μg/mL of fibronectin. The spheroids were imaged on days 0, 3, 5, 7, and 10 to determine the invasion distance into the ECM (Fig. 5H and S4C). The results show that α5β1 expression dramatically enhances cell invasion (Fig. 5I). Results from Fig. 5, suggest that ITGA5 expression enhances migration within a multicellular spheroid, allowing cells to more quickly access the cell-ECM boundary where ITGA5 expression promotes invasion into the surrounding matrix.

ITGA5 promotes metastasis of MDA-MB-231 cells

Since migration and invasion are two critical steps in the metastatic cascade, ITGA5 knockdown subclones were injected into the mammary fat pad (MFP) of NOD-SCID mice to assess tumor growth and metastasis. The *in vitro* and *in vivo* proliferation rates of the knockdown and control subclones were similar and tumors formed at a similar rate (Fig. 6A and Fig. S5A). We also compared the overall metastatic burden resulting from control tumors or tumors lacking ITGA5 by isolating genomic DNA from the mouse lung for analysis of human DNA by quantitative real-time PCR (qPCR) (Fig. 6B). Inhibition of ITGA5 expression in tumors significantly decreased lung metastasis. Lung metastasis was also assessed histologically by hematoxylin and eosin staining (Fig. 6C). The number of metastatic foci per field of view in each section (Fig. 6D) confirmed the qPCR results (Fig. 6B).

We assessed breast cancer cell infiltration of the ipsilateral axillary lymph node by immunohistochemistry using an antibody that specifically recognizes human vimentin. The lymph nodes of mice bearing control tumors were enlarged and completely infiltrated with breast cancer cells, whereas normal follicular structure and size were maintained in mice bearing ITGA5-knockdown tumors (Fig. 6E-F and Fig. S5B).

ITGA5 promotes metastasis in an immunocompetent mouse model of breast cancer

To investigate the role of ITGA5 in an immunocompetent model, we used 4T1 mouse mammary carcinoma cells, which form primary tumors and metastases similar to human TNBC after implantation into the MFP of syngeneic BALB/c mice. We generated 4T1 subclones that were stably transfected with a vector encoding NTC shRNA or shRNA that inhibited the expression of mouse ITGA5 (shA5-1, shA5-2) (Fig. 7A). After orthotopic implantation in the MFP of female BALB/c mice, the growth of primary tumors derived from shA5-1 or shA5-2 subclones did not show a significant decrease in growth compared to tumors derived from NTC subclone cells (Fig. 7B). The number of metastatic nodules in lungs (Fig. 7C-E) harvested from mice implanted with shA5 cells were significantly decreased compared to mice implanted with NTC cells whereas metastatic foci in axillary lymph nodes were similar between groups (Fig. 7F). Interestingly, the lymph node volume of non-tumor bearing BALB/c mice are 2-3 times larger than lymph nodes from non-tumor bearing NOD-SCID mice. Taken together this suggests that decreased lymph node seeding of ITGA5-deficient cells only occurs in the absence of competent immune cells.

To determine if our results were relevant for human cancer, we analyzed microarray expression data obtained from over 1,800 primary human breast cancers, stratifying patients by high (above the median level) or low (below the median level) expression of *ITGA5* or *ITGB1* for survival analysis. High ITGA5 but not ITGB1 mRNA levels were associated with decreased patient survival (Fig. 7G and Fig. S6A), and was independent of estrogen receptor or lymph node status (Fig. S6B). By further stratifying patients into basal, luminal and $HER2^+$ subtypes based on the PAM50 score for each patient (38), we found that only patients with basal or $HER2^+$ subtypes of breast cancer showed a significant correlation between increased ITGA5 expression and patient mortality (Fig. 7H-I). Based on results from chi-square testing, ITGA5 expression is not associated with lymph node status in this data set. Thus, expression levels of ITGA5 are prognostic for distant metastasis free survival in patients but not lymph node infiltration, which is consistent with the observed role of ITGA5 in promoting lung metastasis in orthotopic transplantation models of TNBC.

Discussion

Hypoxia selectively induces integrin expression in breast cancer cells

Intratumoral hypoxia induces the expression of HIF-1α, which is associated with an increased risk of metastasis, relapse, and mortality in clinical studies (23). Many studies have highlighted the role of hypoxia and HIF-1 in inducing the expression of multiple genes that are involved in ECM processing and promote metastasis in tumor models (18-20,23,52-56), suggesting that ECM-binding proteins, such as integrins, could be induced under hypoxic conditions. Given that several integrin inhibitors are advancing through clinical trials, identifying which integrin is induced by hypoxia could provide a useful approach to specifically target hypoxic cells. Therefore, we investigated the role of hypoxia and HIFs in the regulation of each individual integrin subunit. Our results showed that ITGA1, ITGA5, ITGA11, and ITGB1 were well correlated with a HIF meta-gene signature. Surprisingly, ITGA1, ITGB1 and ITGA11 were induced in less than half of the cell lines tested. ITGA5 mRNA expression was (a) induced in 19 out of 20 breast cancer cell lines tested; (b) prognostic for patient survival; and (c) increased 50 fold in basal compared to luminal breast cancers. The findings suggest a unique and potentially complex pattern of hypoxia-regulated induction of integrin subunits which can only be recognized by assessing a large panel of cell lines to determine the robustness of the hypoxic response across cell lines which harbor extensive genetic and phenotype differences.

ITGA5 promotes 3D motility and invasion

ITGA5 modulated single cell migration within a complex multicellular spheroid as well as single cell migration within 3D collagen-fibronectin gels but did not alter cell migration in 2D. The difference between 2D and 3D motility has been observed previously in multiple contexts. For example, previous studies suggest that migrating breast, pancreatic, and prostate cancer cells do not display lamellipodial structures in 3D but instead have unique dendritic protrusions (57). Recent work shows that Rab coupling protein (RCP, also known as Rab11-FIP1) interacts with, and controls, the recycling of α5β1. In 3D matrices, RCP–α5β1 trafficking increased local invasion by enhancing dynamic actin spike protrusions unique to cells in 3D to promote migration (58). Our previous results have shown that

hypoxia induces RhoA and ROCK1 expression to enhance motility under hypoxic conditions (59). Determining how and if ITGA5 signals to RhoA and ROCK1 in a complex 3D environment may increase our understanding of the functional effects of the coordinate regulation of ECM, integrins, and the Rho signaling pathway in the hypoxic tumor microenvironment.

Mechanisms of ITGA5 and ITGB1 induction by hypoxic conditions

We determined that HIF-1 and HIF-2 bind to an HRE in the *ITGA5* gene to activate its transcription, leading to increased ITGA5 mRNA and protein expression. Interestingly, HIF-1α, but not HIF-2α, was also required for the hypoxia-induced expression of *ITGB1* (the obligate partner of ITGA1). The findings suggest that integrin inhibitors, which are being tested in clinical trials (28,60), may hold promise for patients with hypoxic tumors and patients with increased levels of ITGA5 due to oncogene activation by ERBB2 (61), c-Myc (62), or by miRNA regulation (63). ATN-161 (Ac-PHSCN-NH2), a peptide that binds to α5β1 and αvβ3, was shown to block breast cancer growth and bone colonization after intracardiac injection of MDA-MB-231 cells (64). Preclinical studies assessing liver and prostate metastasis also demonstrated a benefit using ATN-161 (65,66). Both ATN-161 and volociximab, a monoclonal antibody that blocks α5β1, demonstrated good tolerability in phase I and II trials (67,68).

In addition to α5β1, blocking integrin αv using Intetumumab, a monoclonal antibody with encouraging results in Phase I and II trials, has been shown to prevent brain metastasis in a 231BR-HER2 hematogenous breast cancer to brain-metastasis model. Cilengitide, an inhibitor of αvβ3 and αvβ5, was the first integrin inhibitor to reach phase III clinical trials (60). In mouse models of breast to bone metastases, abrogating integrin β3 expression prevented bone metastasis. In our studies, we did not observe induction of αv or β3 expression under hypoxic conditions. However, hypoxia has been shown to regulate αv and β3 transcription in endothelial cells (31) and $\alpha v\beta_3$ cell surface expression in melanoma cells (32). It is also possible that additional integrin subunits may play a role in modulating metastasis, for example the laminin binding integrin α6β1 has been shown to sustain the stem-like state of breast cancer cells (69). Integrin α6 was not induced by hypoxia in our studies.

Given our finding that inhibition of ITGA5 expression prevents spontaneous lung metastasis in mouse models and several pathways converge to promote ITGA5 expression during tumor progression, and recent evidence suggesting that reducing ITGA5 levels in the presence of a PI3K inhibitor (navitoclax) can enhance apoptosis in PTEN-mutant cancer cells (70) suggest that further studies are warranted. Integrin blockers should be considered as potential therapeutics, especially in patients with hypoxic tumors.

Supplementary Material

Refer to Web version on PubMed Central for supplementary material.

Acknowledgments

We thank Karen Padgett of Novus Biologicals for providing HIF-2α antibodies. This work was supported by NCI grant U54-CA143868 (GLS and DW) and R00-CA181352 (DMG).

References

1. Dewhirst MW. Intermittent hypoxia furthers the rationale for hypoxia-inducible factor-1 targeting. Cancer Res. 2007; 67(3):854–5. [PubMed: 17283112]
2. Brahimi-Horn MC, Chiche J, Pouyssegur J. Hypoxia and cancer. J Mol Med. 2007; 85(12):1301–7. [PubMed: 18026916]
3. Gillies RJ, Gatenby RA. Hypoxia and adaptive landscapes in the evolution of carcinogenesis. Cancer Metastasis Rev. 2007; 26(2):311–7. [PubMed: 17404691]
4. Semenza GL. Targeting HIF-1 for cancer therapy. Nat Rev Cancer. 2003; 3(10):721–32. [PubMed: 13130303]
5. Semenza GL. Defining the role of hypoxia-inducible factor 1 in cancer biology and therapeutics. Oncogene. 2010; 29(5):625–34. [PubMed: 19946328]
6. Wang GL, Jiang BH, Rue EA, Semenza GL. Hypoxia-inducible factor 1 is a basic-helix-loop-helix-PAS heterodimer regulated by cellular O_2 tension. Proc Natl Acad Sci U S A. 1995; 92(12):5510–4. [PubMed: 7539918]
7. Helczynska K, Larsson AM, Holmquist Mengelbier L, Bridges E, Fredlund E, Borgquist S, et al. Hypoxia-inducible factor-2α correlates to distant recurrence and poor outcome in invasive breast cancer. Cancer Res. 2008; 68(22):9212–20. [PubMed: 19010893]
8. Hiraga T, Kizaka-Kondoh S, Hirota K, Hiraoka M, Yoneda T. Hypoxia and hypoxiainducible factor-1 expression enhance osteolytic bone metastases of breast cancer. Cancer Res. 2007; 67(9): 4157–63. [PubMed: 17483326]
9. Li L, Lin X, Staver M, Shoemaker A, Semizarov D, Fesik SW, et al. Evaluating hypoxia-inducible factor-1α as a cancer therapeutic target via inducible RNA interference in vivo. Cancer Res. 2005; 65(16):7249–58. [PubMed: 16103076]
10. Liao D, Corle C, Seagroves TN, Johnson RS. Hypoxia-inducible factor-1α is a key regulator of metastasis in a transgenic model of cancer initiation and progression. Cancer Res. 2007; 67(2): 563–72. [PubMed: 17234764]
11. Zhang H, Wong CC, Wei H, Gilkes DM, Korangath P, Chaturvedi P, et al. HIF-1-dependent expression of angiopoietin-like 4 and L1CAM mediates vascular metastasis of hypoxic breast cancer cells to the lungs. Oncogene. 2012; 31(14):1757–70. [PubMed: 21860410]
12. Wong CC, Gilkes DM, Zhang H, Chen J, Wei H, Chaturvedi P, et al. Hypoxia-inducible factor 1 is a master regulator of breast cancer metastatic niche formation. Proc Natl Acad Sci U S A. 2011; 108(39):16369–74. [PubMed: 21911388]
13. Bos R, van der Groep P, Greijer AE, Shvarts A, Meijer S, Pinedo HM, et al. Levels of hypoxia-inducible factor-1α independently predict prognosis in patients with lymph node negative breast carcinoma. Cancer. 2003; 97(6):1573–81. [PubMed: 12627523]
14. Schindl M, Schoppmann SF, Samonigg H, Hausmaninger H, Kwasny W, Gnant M, et al. Overexpression of hypoxia-inducible factor 1α is associated with an unfavorable prognosis in lymph node-positive breast cancer. Clin Cancer Res. 2002; 8(6):1831–7. [PubMed: 12060624]
15. Generali D, Berruti A, Brizzi MP, Campo L, Bonardi S, Wigfield S, et al. Hypoxiainducible factor-1α expression predicts a poor response to primary chemoendocrine therapy and disease-free survival in primary human breast cancer. Clin Cancer Res. 2006; 12(15):4562–8. [PubMed: 16899602]
16. Yamamoto Y, Ibusuki M, Okumura Y, Kawasoe T, Kai K, Iyama K, et al. Hypoxiainducible factor 1α is closely linked to an aggressive phenotype in breast cancer. Breast Cancer Res Treat. 2008; 110(3):465–75. [PubMed: 17805961]
17. Dales JP, Garcia S, Meunier-Carpentier S, Andrac-Meyer L, Haddad O, Lavaut MN, et al. Overexpression of hypoxia-inducible factor HIF-1α predicts early relapse in breast cancer:

retrospective study in a series of 745 patients. Int J Cancer. 2005; 116(5):734–9. [PubMed: 15849727]

18. Gilkes DM, Bajpai S, Chaturvedi P, Wirtz D, Semenza GL. Hypoxia-inducible factor 1 (HIF-1) promotes extracellular matrix remodeling under hypoxic conditions by inducing P4HA1, P4HA2, and PLOD2 expression in fibroblasts. J Biol Chem. 2013; 288(15):10819–29. [PubMed: 23423382]
19. Gilkes DM, Bajpai S, Wong CC, Chaturvedi P, Hubbi ME, Wirtz D, et al. Procollagen lysyl hydroxylase 2 is essential for hypoxia-induced breast cancer metastasis. Mol Cancer Res. 2013; 11(5):456–66. [PubMed: 23378577]
20. Gilkes DM, Chaturvedi P, Bajpai S, Wong CC, Wei H, Pitcairn S, et al. Collagen prolyl hydroxylases are essential for breast cancer metastasis. Cancer Res. 2013; 73(11):3285–96. [PubMed: 23539444]
21. Danen EH, van Rheenen J, Franken W, Huveneers S, Sonneveld P, Jalink K, et al. Integrins control motile strategy through a Rho-cofilin pathway. J Cell Biol. 2005; 169(3):515–26. [PubMed: 15866889]
22. Vleminckx K, Vakaet L Jr, Mareel M, Fiers W, van Roy F. Genetic manipulation of Ecadherin expression by epithelial tumor cells reveals an invasion suppressor role. Cell. 1991; 66(1):107–19. [PubMed: 2070412]
23. Gilkes DM, Semenza GL, Wirtz D. Hypoxia and the extracellular matrix: drivers of tumour metastasis. Nat Rev Cancer. 2014; 14(6):430–9. [PubMed: 24827502]
24. Frantz C, Stewart KM, Weaver VM. The extracellular matrix at a glance. J Cell Sci. 2010; 123(Pt 24):4195–200. [PubMed: 21123617]
25. Lu P, Weaver VM, Werb Z. The extracellular matrix: a dynamic niche in cancer progression. J Cell Biol. 2012; 196(4):395–406. [PubMed: 22351925]
26. van der Flier A, Sonnenberg A. Function and interactions of integrins. Cell and tissue research. 2001; 305(3):285–98. [PubMed: 11572082]
27. Hynes RO. Integrins: bidirectional, allosteric signaling machines. Cell. 2002; 110(6):673–87. [PubMed: 12297042]
28. Desgrosellier JS, Cheresh DA. Integrins in cancer: biological implications and therapeutic opportunities. Nat Rev Cancer. 2010; 10(1):9–22. [PubMed: 20029421]
29. Gilcrease MZ. Integrin signaling in epithelial cells. Cancer Lett. 2007; 247(1):1–25. [PubMed: 16725254]
30. Keely S, Glover LE, MacManus CF, Campbell EL, Scully MM, Furuta GT, et al. Selective induction of integrin beta1 by hypoxia-inducible factor: implications for wound healing. FASEB J. 2009; 23(5):1338–46. [PubMed: 19103643]
31. Walton HL, Corjay MH, Mohamed SN, Mousa SA, Santomenna LD, Reilly TM. Hypoxia induces differential expression of the integrin receptors alpha(vbeta3) and alpha(vbeta5) in cultured human endothelial cells. J Cell Biochem. 2000; 78(4):674–80. [PubMed: 10861864]
32. Cowden Dahl KD, Robertson SE, Weaver VM, Simon MC. Hypoxia-inducible factor regulates αvβ3 integrin cell surface expression. Mol Biol Cell. 2005; 16(4):1901–12. [PubMed: 15689487]
33. Kong T, Eltzschig HK, Karhausen J, Colgan SP, Shelley CS. Leukocyte adhesion during hypoxia is mediated by HIF-1-dependent induction of beta2 integrin gene expression. Proc Natl Acad Sci U S A. 2004; 101(28):10440–5. [PubMed: 15235127]
34. Kong T, Scully M, Shelley CS, Colgan SP. Identification of Pur α as a new hypoxia response factor responsible for coordinated induction of the β 2 integrin family. J Immunol. 2007; 179(3):1934–41. [PubMed: 17641060]
35. Koike T, Kimura N, Miyazaki K, Yabuta T, Kumamoto K, Takenoshita S, et al. Hypoxia-induces adhesion molecules on cancer cells: A missing link between Warburg effect and induction of selectin-ligand carbohydrates. Proc Natl Acad Sci U S A. 2004; 101(21):8132–7. [PubMed: 15141079]
36. Saller MM, Prall WC, Docheva D, Schonitzer V, Popov T, Anz D, et al. Increased stemness and migration of human mesenchymal stem cells in hypoxia is associated with altered integrin expression. Biochem Biophys Res Commun. 2012; 423(2):379–85. [PubMed: 22664105]

37. Comprehensive molecular portraits of human breast tumours. Nature. 2012; 490(7418):61–70. [PubMed: 23000897]
38. Ringner M, Fredlund E, Hakkinen J, Borg A, Staaf J. GOBO: gene expression-based outcome for breast cancer online. PLoS One. 2011; 6(3):e17911. [PubMed: 21445301]
39. Zhang H, Wong C, Wei H, Gilkes D, Korangath P, Chaturvedi P, et al. HIF-1-dependent expression of angiopoietin-like 4 and L1CAM mediates vascular metastasis of hypoxic breast cancer cells to the lungs. Oncogene. 2011; 31(14):1757–70. [PubMed: 21860410]
40. Hu H, Takano N, Xiang L, Gilkes DM, Luo W, Semenza GL. Hypoxia-inducible factors enhance glutamate signaling in cancer cells. Oncotarget. 2014; 5(19):8853–68. [PubMed: 25326682]
41. Wu PH, Giri A, Wirtz D. Statistical analysis of cell migration in 3D using the anisotropic persistent random walk model. Nat Protoc. 2015; 10(3):517–27. [PubMed: 25719270]
42. Jimenez Valencia AM, Wu PH, Yogurtcu ON, Rao P, DiGiacomo J, Godet I, et al. Collective cancer cell invasion induced by coordinated contractile stresses. Oncotarget. 2015; 6(41):43438–51. [PubMed: 26528856]
43. Samanta D, Gilkes DM, Chaturvedi P, Xiang L, Semenza GL. Hypoxia-inducible factors are required for chemotherapy resistance of breast cancer stem cells. Proc Natl Acad Sci U S A. 2014; 111(50):E5429–38. [PubMed: 25453096]
44. Kim DH, Wirtz D. Focal adhesion size uniquely predicts cell migration. FASEB J. 2013; 27(4): 1351–61. [PubMed: 23254340]
45. Kim DH, Wirtz D. Predicting how cells spread and migrate: Focal adhesion size does matter. Cell Adh Migr. 2013; 7(3):293–6. [PubMed: 23628962]
46. Wu PH, Giri A, Sun SX, Wirtz D. Three-dimensional cell migration does not follow a random walk. Proc Natl Acad Sci U S A. 2014; 111(11):3949–54. [PubMed: 24594603]
47. Naba A, Clauser KR, Lamar JM, Carr SA, Hynes RO. Extracellular matrix signatures of human mammary carcinoma identify novel metastasis promoters. eLife. 2014; 3:e01308. [PubMed: 24618895]
48. Conklin MW, Eickhoff JC, Riching KM, Pehlke CA, Eliceiri KW, Provenzano PP, et al. Aligned collagen is a prognostic signature for survival in human breast carcinoma. Am J Pathol. 2011; 178(3):1221–32. [PubMed: 21356373]
49. Lyons TR, O'Brien J, Borges VF, Conklin MW, Keely PJ, Eliceiri KW, et al. Postpartum mammary gland involution drives progression of ductal carcinoma in situ through collagen and COX-2. Nat Med. 2011; 17(9):1109–15. [PubMed: 21822285]
50. Schedin P, Keely PJ. Mammary gland ECM remodeling, stiffness, and mechanosignaling in normal development and tumor progression. Cold Spring Harb Perspect Biol. 2011; 3(1):a003228. [PubMed: 20980442]
51. Bae YK, Kim A, Kim MK, Choi JE, Kang SH, Lee SJ. Fibronectin expression in carcinoma cells correlates with tumor aggressiveness and poor clinical outcome in patients with invasive breast cancer. Human pathology. 2013; 44(10):2028–37. [PubMed: 23684510]
52. Erler JT, Bennewith KL, Nicolau M, Dornhofer N, Kong C, Le QT, et al. Lysyl oxidase is essential for hypoxia-induced metastasis. Nature. 2006; 440(7088):1222–6. [PubMed: 16642001]
53. Wong CC, Zhang H, Gilkes DM, Chen J, Wei H, Chaturvedi P, et al. Inhibitors of hypoxia-inducible factor 1 block breast cancer metastatic niche formation and lung metastasis. J Mol Med (Berl). 2012; 90(7):803–15. [PubMed: 22231744]
54. Cox TR, Bird D, Baker AM, Barker HE, Ho MW, Lang G, et al. LOX-mediated collagen crosslinking is responsible for fibrosis-enhanced metastasis. Cancer Res. 2013; 73(6):1721–32. [PubMed: 23345161]
55. Erler JT, Bennewith KL, Cox TR, Lang G, Bird D, Koong A, et al. Hypoxia-induced lysyl oxidase is a critical mediator of bone marrow cell recruitment to form the premetastatic niche. Cancer Cell. 2009; 15(1):35–44. [PubMed: 19111879]
56. Wong CC-L, Gilkes DM, Zhang H, Chen J, Wei H, Chaturvedi P, et al. Hypoxiainducible factor 1 is a master regulator of breast cancer metastatic niche formation. Proc Natl Acad Sci U S A. 2011; 108(39):16369–74. [PubMed: 21911388]

57. Giri A, Bajpai S, Trenton N, Jayatilaka H, Longmore GD, Wirtz D. The Arp2/3 complex mediates multigeneration dendritic protrusions for efficient 3-dimensional cancer cell migration. FASEB J. 2013; 27(10):4089–99. [PubMed: 23796785]
58. Paul NR, Allen JL, Chapman A, Morlan-Mairal M, Zindy E, Jacquemet G, et al. α5β1 integrin recycling promotes Arp2/3-independent cancer cell invasion via the formin FHOD3. J Cell Biol. 2015; 210(6):1013–31. [PubMed: 26370503]
59. Gilkes DM, Xiang L, Lee SJ, Chaturvedi P, Hubbi ME, Wirtz D, et al. Hypoxia-inducible factors mediate coordinated RhoA-ROCK1 expression and signaling in breast cancer cells. Proceedings of the National Academy of Sciences. 2014; 111(3):E384–E93.
60. Stupp R, Hegi ME, Gorlia T, Erridge SC, Perry J, Hong YK, et al. Cilengitide combined with standard treatment for patients with newly diagnosed glioblastoma with methylated MGMT promoter (CENTRIC EORTC 26071-22072 study): a multicentre, randomised, open-label, phase 3 trial. Lancet Oncol. 2014; 15(10):1100–8. [PubMed: 25163906]
61. Spangenberg C, Lausch EU, Trost TM, Prawitt D, May A, Keppler R, et al. ERBB2-Mediated Transcriptional Up-regulation of the α5β1 Integrin Fibronectin Receptor Promotes Tumor Cell Survival Under Adverse Conditions. Cancer Res. 2006; 66(7):3715–25. [PubMed: 16585198]
62. Damiano L, Stewart KM, Cohet N, Mouw JK, Lakins JN, Debnath J, et al. Oncogenic targeting of BRM drives malignancy through C/EBPbeta-dependent induction of alpha5 integrin. Oncogene. 2014; 33(19):2441–53. [PubMed: 23770848]
63. Orso F, Quirico L, Virga F, Penna E, Dettori D, Cimino D, et al. miR-214 and miR-148b Targeting Inhibits Dissemination of Melanoma and Breast Cancer. Cancer Res. 2016; 76(17):5151–62. [PubMed: 27328731]
64. Khalili P, Arakelian A, Chen G, Plunkett ML, Beck I, Parry GC, et al. A non-RGD-based integrin binding peptide (ATN-161) blocks breast cancer growth and metastasis in vivo. Mol Cancer Ther. 2006; 5(9):2271–80. [PubMed: 16985061]
65. Stoeltzing O, Liu W, Reinmuth N, Fan F, Parry GC, Parikh AA, et al. Inhibition of integrin α5β1 function with a small peptide (ATN-161) plus continuous 5-FU infusion reduces colorectal liver metastases and improves survival in mice. Int J Cancer. 2003; 104(4):496–503. [PubMed: 12584749]
66. Livant DL, Brabec RK, Pienta KJ, Allen DL, Kurachi K, Markwart S, et al. Anti-invasive, antitumorigenic, and antimetastatic activities of the PHSCN sequence in prostate carcinoma. Cancer Res. 2000; 60(2):309–20. [PubMed: 10667582]
67. Cianfrocca M, Kimmel K, Gallo J, Cardoso T, Brown M, Hudes G, et al. Phase 1 trial of the antiangiogenic peptide ATN-161 (Ac-PHSCN-NH2), a beta integrin antagonist, in patients with solid tumours. British journal of cancer. 2006; 94(11):1621–6. [PubMed: 16705310]
68. Barkan D, Chambers AF. beta1-integrin: a potential therapeutic target in the battle against cancer recurrence. Clin Cancer Res. 2011; 17(23):7219–23. [PubMed: 21900388]
69. Chang C, Goel HL, Gao H, Pursell B, Shultz LD, Greiner DL, et al. A laminin 511 matrix is regulated by TAZ and functions as the ligand for the alpha6Bbeta1 integrin to sustain breast cancer stem cells. Genes Dev. 2015; 29(1):1–6. [PubMed: 25561492]
70. Ren W, Joshi R, Mathew P. Synthetic Lethality in PTEN-Mutant Prostate Cancer Is Induced by Combinatorial PI3K/Akt and BCL-XL Inhibition. Mol Cancer Res. 2016; 14(12):1176–81. [PubMed: 27590631]

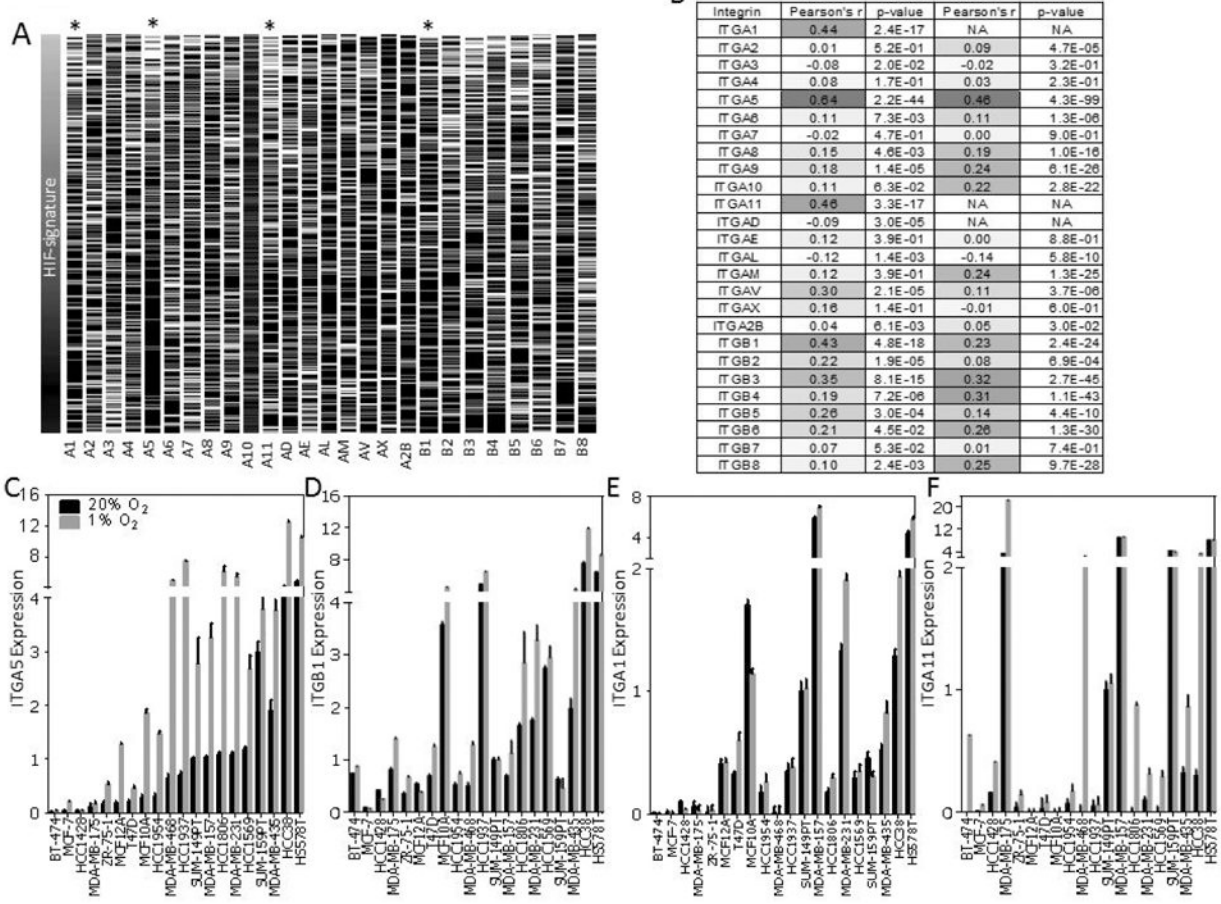

Integrin	TCGA Pearson's r	TCGA p-value	GOBO Pearson's r	GOBO p-value
ITGA1	0.44	2.4E-17	NA	NA
ITGA2	0.01	5.2E-01	0.09	4.7E-05
ITGA3	-0.08	2.0E-02	-0.02	3.2E-01
ITGA4	0.08	1.7E-01	0.03	2.3E-01
ITGA5	0.64	2.2E-44	0.46	4.3E-99
ITGA6	0.11	7.3E-03	0.11	1.3E-06
ITGA7	-0.02	4.7E-01	0.00	9.0E-01
ITGA8	0.15	4.6E-03	0.19	1.0E-16
ITGA9	0.18	1.4E-05	0.24	6.1E-26
ITGA10	0.11	6.3E-02	0.22	2.8E-22
ITGA11	0.46	3.3E-17	NA	NA
ITGAD	-0.09	3.0E-05	NA	NA
ITGAE	0.12	3.9E-01	0.00	8.8E-01
ITGAL	-0.12	1.4E-03	-0.14	5.8E-10
ITGAM	0.12	3.9E-01	0.24	1.3E-25
ITGAV	0.30	2.1E-05	0.11	3.7E-06
ITGAX	0.16	1.4E-01	-0.01	6.0E-01
ITGA2B	0.04	6.1E-03	0.05	3.0E-02
ITGB1	0.43	4.8E-18	0.23	2.4E-24
ITGB2	0.22	1.9E-05	0.08	6.9E-04
ITGB3	0.35	8.1E-15	0.32	2.7E-45
ITGB4	0.19	7.2E-06	0.31	1.1E-43
ITGB5	0.26	3.0E-04	0.14	4.4E-10
ITGB6	0.21	4.5E-02	0.26	1.3E-30
ITGB7	0.07	5.3E-02	0.01	7.4E-01
ITGB8	0.10	2.4E-03	0.25	9.7E-28

Figure 1.

Integrin expression in breast tumors and breast cancer cell lines. **A**, heat map representing the mRNA transcript level of integrin gene expression in each tumor (n = 597) in the TCGA Breast Cancer Data Set ordered by low to high expression level of the hypoxic gene signature score (see also Fig. S1a). black = high, white = low. **B**, Pearson's product-moment correlation coefficient (r = −1 to 1) which describes the correlation and *P* value to compare the hypoxic gene signature score and the expression of each integrin subunit for samples in the TCGA dataset shown in **(A)** and tumors (n = 1880) in the GOBO dataset. **C-F,** qPCR to determine ITGA5 (**C**), ITGB1 (**D**), ITGA1 (**E**), and ITGA11 (**F**) mRNA levels in 20 breast cancer cell lines, normalized to mean value for SUM-149PT cells at 20% O_2.

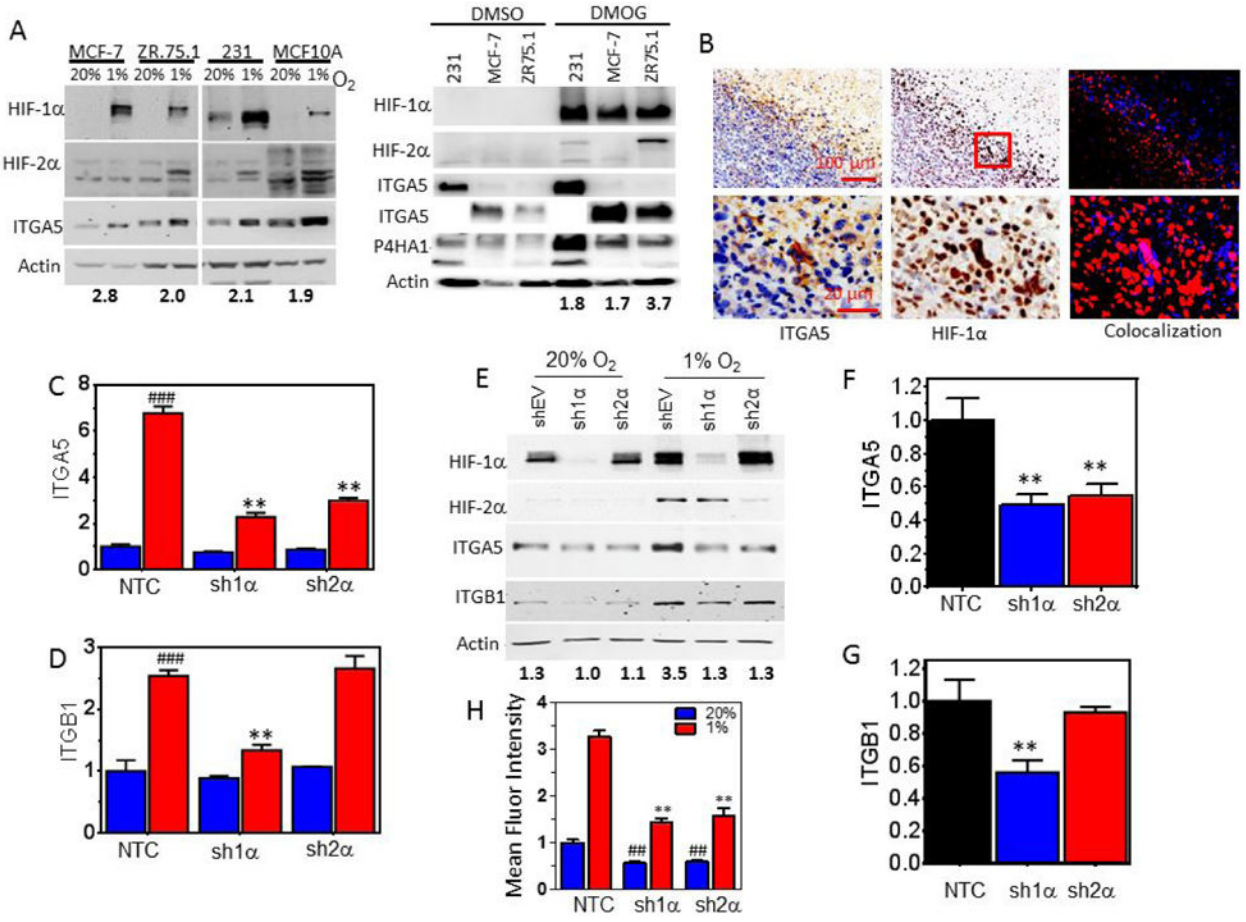

Figure 2.

HIF-1α and HIF-2α are required for hypoxia-induced *ITGA5* expression. **A,** Immunoblot assays were performed using lysates prepared from MCF-7, ZR.75.1, MDA-MB-231 (231) and MCF10A cells exposed to 20% or 1% O_2 for 48 h (left panel) or 1mM of DMOG or an equal volume of DMSO (right panel). The fold increase of ITGA5 (normalized by actin) protein under 1% O_2 compared to 20% O_2 conditions is denoted beneath the immunoblot. Note: 10× lower exposure times for ITGA5 were used for 231 and MCF10A cells as compared to MCF-7 and ZR75.1 cells. **B,** Immunohistochemical staining for HIF-1α and ITGA5 on sections of MDA-MB-231 orthotopic breast tumors. Images were deconvoluted and pseudo-colored for ITGA5 (red) and HIF-1α (blue) staining to assess colocalization (right). **C-D,** ITGA5 **(C)** and ITGB1 **(D)** mRNA levels were analyzed by qPCR in MDA-MB-231 subclones, which were stably transfected with a non-targeting control shRNA vector (NTC) or vector encoding either HIF-1α shRNA (sh1α) or HIF-2α shRNA (sh2α) and exposed to 20% or 1% O_2 for 24 h (mean ± SEM, n = 3-5); $^{**}P < 0.01$ versus NTC at 1% O_2 or $^{\#\#\#}P < 0.001$ versus NTC at 20% O_2 (twoway ANOVA with Bonferroni posttest). **E,** Immunoblot assays were performed using lysates prepared from MDA-MB-231 subclones exposed to 20% or 1% O_2 for 48 hours. ITGA5 densitometry measurements normalized by actin levels are denoted for each sample. **F-G,** ITGA5 **(F)** and ITGB1 **(G)** mRNA levels were analyzed in tumors established with MDA-MB-231 subclones (mean ± SEM, n = 5); $^{*}P < 0.05$, $^{**}P < 0.01$ versus NTC (one-way ANOVA with Bonferroni

posttest). **(H)** Flow cytometry analysis to assess the fluorescent intensity of ITGA5 antibody binding to MDA-MB-231 cells was conducted for subclones exposed to 20% or 1% O_2 for 48 h (mean ± SEM, n = 3); ** $P < 0.01$ versus NTC at 1% O_2; ## $P < 0.01$ versus NTC at 20% O_2 (two-way ANOVA with Bonferroni posttest for multiple comparisons).

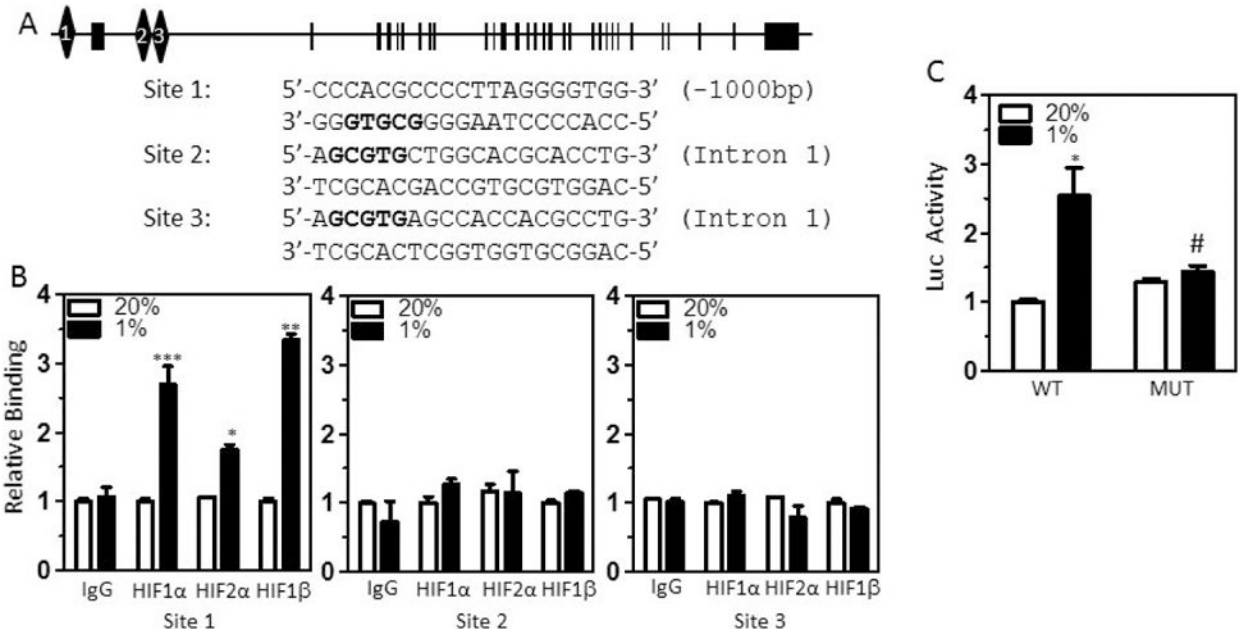

Figure 3.

ITGA5 is a transcriptional target of HIF-1 and HIF-2. **A,** Candidate HIF binding sites (diamonds) were identified in the 5′-flanking region and intron 1 of the human *ITGA5* gene (exon 1 shown as rectangle). **B,** MDA-MB-231 cells were incubated at 20% or 1% O_2 for 18 h, and chromatin immunoprecipitation (ChIP) assays were performed using IgG or antibodies against HIF-1α, HIF-2α or HIF-1β. Specific primers flanking candidate HIF binding sites were used for qPCR, and values were normalized to cells exposed to 20% O_2 (mean ± SEM; n = 3). $^{*}P < 0.05$, $^{***}P < 0.001$ vs. 20% O_2 (Student's *t* test). **C,** A wild type (WT) or mutant (MUT) 60-bp fragment surrounding the putative HIF binding site in the 5′-flanking region of *ITGA5* was cloned into the pGL2-Promoter luciferase reporter plasmid and firefly luciferase activity (Luc) was determined in MDA-MB-231 cells. $^{*}P < 0.05$ vs WT at 20% O_2; $^{\#}P < 0.05$ vs WT at 1% O_2 (two-way ANOVA with Bonferroni posttest).

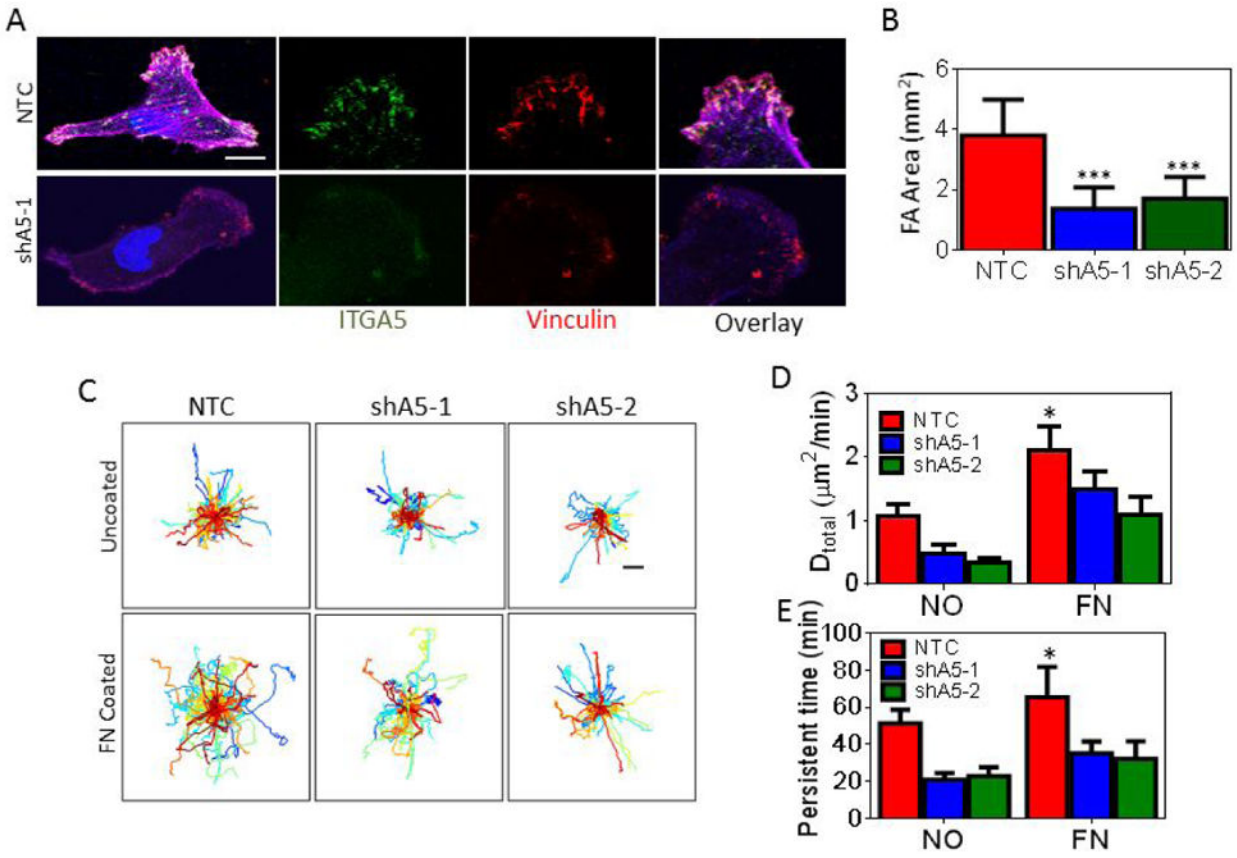

Figure 4.

Inhibition of ITGA5 expression affects cell motility in 2D. **A,** Non-targeting control (NTC) or ITGA5-knockdown (shA5-1 and shA5-2) MDA-MB-231 subclones were labeled with antibodies against ITGA5 (green) and vinculin (red), and stained with DAPI (blue) followed by fluorescence imaging. Scale bar = 10 μm. **B,** The focal adhesion (FA) area (vinculin staining) was measured using image analysis and normalized by cell area. Data are shown as mean ± SEM; n = 15-30 cells. ***$P < 0.001$ vs. NTC (two-way ANOVA with Bonferroni posttest). **C,** Cell trajectories (n = 75-100) are plotted using x,y coordinates obtained at 5-min intervals over a 13-h time course. Scale bar = 40 μm. **D-E,** The diffusivity **(D)** and persistent time **(E)** of subclones migrating on uncoated or fibronectin-coated plates were calculated. Data are shown as mean ± SEM; n = 75-100. *$P < 0.05$ vs. NTC (two-way ANOVA with Bonferroni posttest for all comparisons).

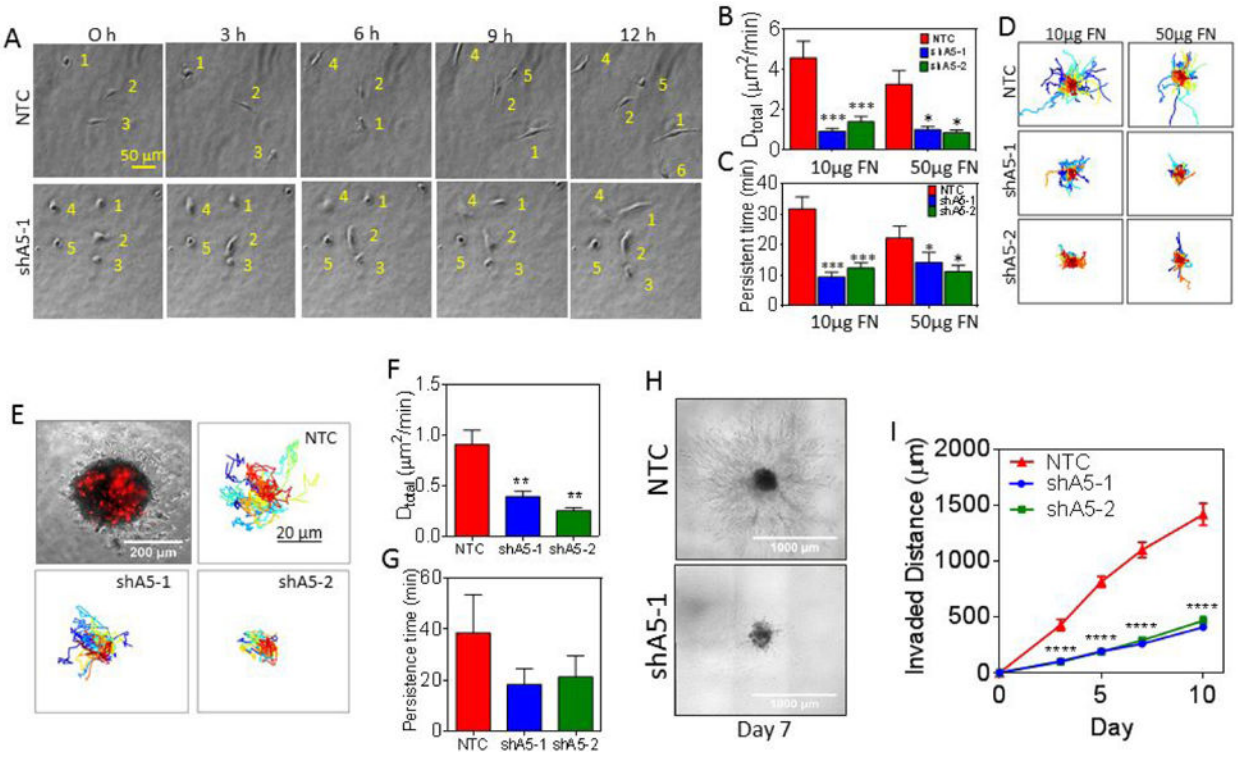

Figure 5.

Knockdown of ITGA5 affects 3D cell motility both as single cells and cells in a multicellular spheroid**. A,** Representative images at 3-h time intervals of cells migrating in a collagen/fibronectin gel. Each cell is numbered to aid visualization. **B-C,** The diffusivity **(B)** and persistent time **(C)** were determined for subclones embedded in 3D collagen gels containing 10 or 50 μg/mL of fibronectin (FN). Data are shown as mean ± SEM; n = 50. ***$P < 0.001$, **$P < 0.01$, *$P < 0.05$ vs. NTC (two-way ANOVA with Bonferroni posttest for all comparisons). **D,** Cell trajectories (n = 75-100) are plotted using x,y coordinates obtained at 5-min intervals over a 13-h time course. **E,** Spheroids containing 1,000 NTC, shA5-1, or shA5-2 cells labeled with a red fluorescent carbocyanine tracer were mixed with 9,000 non-labelled naive cells and embedded into collagen gels containing 50 μg/mL of fibronectin (top left corner). Cell trajectories (n = 40) are plotted using x,y coordinates obtained at 20-min intervals over a 15-h time course. Scale bar = 20 μm. **F-G,** The diffusivity **(F)** and persistent time **(G)** of subclones migrating within spheroids were calculated. Data are shown as mean ± SEM; n = 40. **$P < 0.01$ vs. NTC (one-way ANOVA with Bonferroni posttest for all comparisons). **H-I,** The invasion of tumor spheroids composed of 10,000 NTC, shA5-1 or shA5-2 cells into collagen gels were imaged by phase contrast (**H**) and the invaded distance measured on day 0, 3, 5, 7 and 10 to examine 3D invasion was plotted (**I**) for comparison. Data are shown as mean ± SEM; n = 10 spheroids. ***$P < 0.001$, *$P < 0.05$ vs. NTC (two-way ANOVA with Bonferroni posttest).

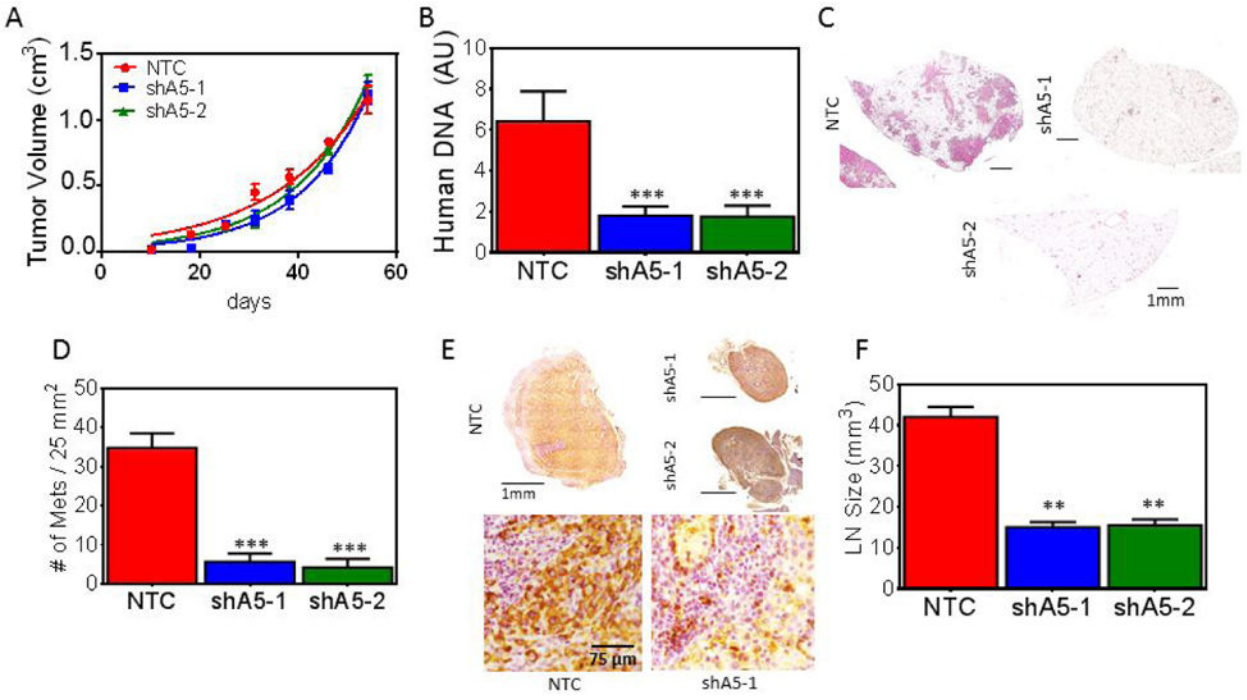

Figure 6.

Inhibition of ITGA5 expression impairs metastasis. **A,** The indicated subclones were injected into the MFP of NOD-SCID mice and tumor volume was plotted versus time. **B,** Human genomic DNA content in mouse lungs was quantified by qPCR for human *HK2* gene sequences. **C,** Lung sections (scale bar = 1 mm) were stained with hematoxylin and eosin to identify metastatic foci. **D,** The number of metastatic foci per 5 × 5 mm lung section was determined (mean ± SEM, n = 5; ***$P < 0.001$, vs. NTC oneway ANOVA with Bonferroni posttest). **E,** Ipsilateral axillary lymph node sections were subjected to immunohistochemistry using an antibody specific for human vimentin. Scale bar = 1 mm (top); scale bar = 75 µm (bottom). **F,** Lymph node volume (V = 0.52 (L*W*[(L+W)/2]) (mean ± SEM, n = 5, **$P < 0.01$, vs. NTC one-way ANOVA).

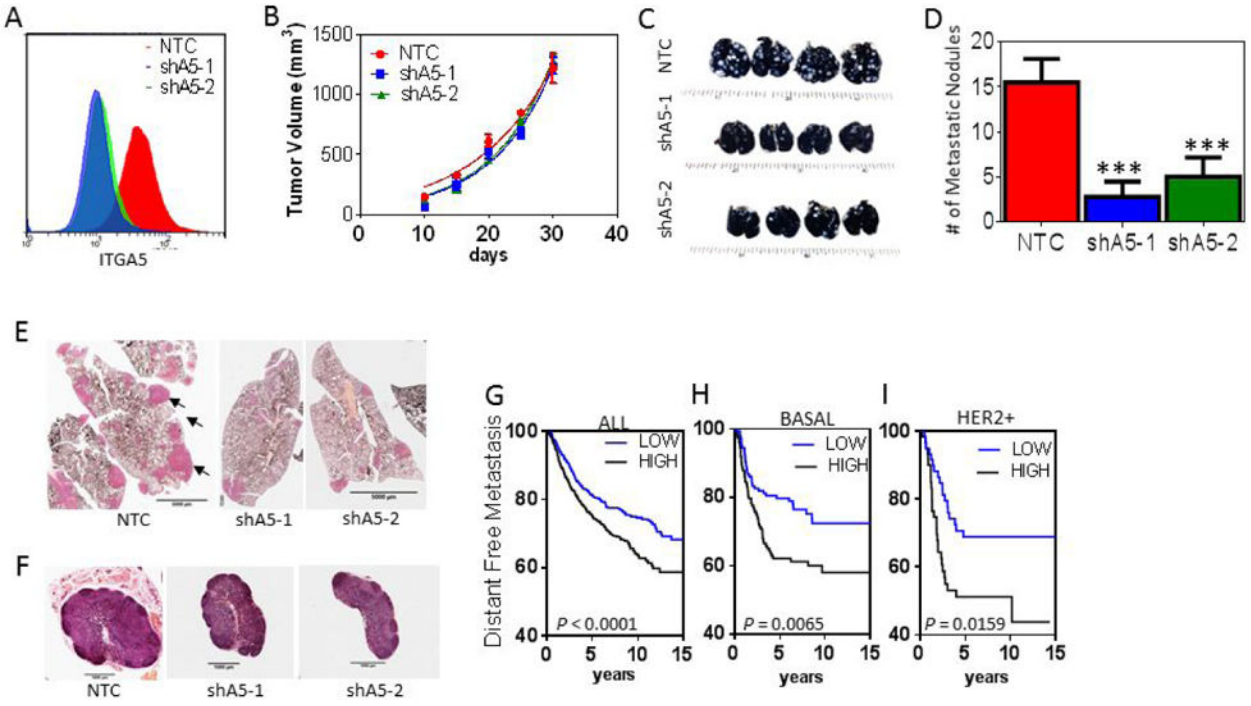

Figure 7.

Inhibition of ITGA5 expression in cancer cells reduces metastasis in an immunocompetent mouse model. 4T1 subclones were implanted in the MFP of syngeneic BALB/c mice. **A,** Histogram showing the fluorescence intensity of ITGA5 staining in NTC, shA5-1, shA5-2 expressing 4T1 cells. **B**, Primary tumor volumes were measured every five days. **C-D,** Whole-mount inflated lungs were stained with India blue dye **(C)** and metastatic nodules (white) were counted **(D)**. E-F, Lung (**E**; scale bar = 5 mm) and lymph node (**F**; scale bar = 1 mm) sections were stained with hematoxylin and eosin. **F,** Kaplan-Meier analysis of distant metastasis-free survival of breast cancer patients (n = 1,881; GOBO database) stratified by ITGA5 mRNA expression above (HIGH) or below (LOW) the median level are presented. **H-I,** The Kaplan–Meier analysis was further stratified for the subset of patients with basal (n = 303) **(H)** or HER2 amplified (**I**) (n =133) breast cancer.